HIV-2 Immature Particle Morphology Provides Insights into Gag Lattice Stability and Virus Maturation

Nathaniel Talledge[1,2,3], Huixin Yang[1,4], Ke Shi[1,3,5], Guichuan Yu[6,8], William G. Arndt[1,7], Luiza M. Mendonça[1,2,^], Hideki Aihara[1,3,5], Louis M. Mansky[1,2,3,4,7]* and Wei Zhang[1,2,3,4,8]*

[1] Institute for Molecular Virology, University of Minnesota – Twin Cities, Minneapolis, MN 55455 USA

[2] Department of Diagnostic and Biological Sciences, University of Minnesota – Twin Cities, Minneapolis, MN 55455 USA

[3] Masonic Cancer Center, University of Minnesota – Twin Cities, Minneapolis, MN 55455 USA

[4] Comparative and Molecular Biosciences Graduate Program, University of Minnesota - Twin Cities, Minneapolis, MN 55455, USA.

[5] Departments of Biochemistry, Molecular Biology and Biophysics, University of Minnesota – Twin Cities, Minneapolis, MN 55455 USA

[6] U of M Informatics Institute, Office of the Vice President for Research, University of Minnesota – Twin Cities, Minneapolis, MN 55455 USA

[7] Biochemistry, Molecular Biology & Biophysics Graduate Program, University of Minnesota – Twin Cities, Minneapolis, MN 55455 USA

[8] Characterization Facility, College of Sciences and Engineering, University of Minnesota – Twin Cities, Minneapolis, MN 55455 USA

* Corresponding authors: mansky@umn.edu, zhangwei@umn.edu

^ Current Address: Division of Structural Biology, Welcome Trust Centre for Human Genetics, University of Oxford, Oxford, OX3 7BN, UK

Abstract

Retrovirus immature particle morphology consists of a membrane enclosed, pleomorphic, spherical and incomplete lattice of Gag hexamers. Previously, we demonstrated that human immunodeficiency virus type 2 (HIV-2) immature particles possess a distinct and extensive Gag lattice morphology. To better understand the nature of the continuously curved hexagonal Gag lattice, we used single particle cryo-electron microscopy to determine the HIV-2 Gag lattice structure for immature virions. The reconstruction map revealed a stable, wineglass-shaped Gag hexamer structure with structural features consistent with other *lentiviral* immature Gag structures. We also solved a 1.98 Å resolution crystal structure of the carboxyl-terminal domain (CTD) of the HIV-2 capsid (CA) protein that identified a structured helix 12 supported via an interaction of helix 10 in the absence of the SP1 region of Gag. Residues at the helix 10-12 interface proved critical in maintaining HIV-2 particle release and infectivity. Taken together, our findings provide evidence for a novel stabilization interface mediated by the HIV-2 CA_{CTD} that delivers important clues for HIV Gag lattice stabilization as well as important insights into virus maturation.

Significance

Retrovirus Gag multimerization triggers the particle assembly, resulting in production of pleomorphic spherical immature virus particles. Previous work has been directed towards defining the amino acid residues critical for intermolecular Gag interactions in the incomplete hexagonal Gag lattice. The structure determination of the HIV-2 Gag hexamer presented here has help define the residues in the HIV-2 capsid that provide important insights into particle assembly, lattice stability and virus maturation.

61 ## Introduction

62

63 Human immunodeficiency virus type 1 (HIV-1) and HIV type 2 (HIV-2) are members of *lentivirus* that
64 cause acquired immunodeficiency syndrome (AIDS) [1]. The assembly of *lentiviruses* occurs at the
65 host cell membrane where Gag oligomerizes and promotes budding of immature viral particles. Gag
66 consists of three major protein domains: the membrane-binding matrix (MA) domain, the capsid (CA)
67 domain that determines the lattice formation in both immature and mature particles, and the genome-
68 binding nucleocapsid (NC) domain [2]. The HIV-1 and HIV-2 Gag proteins also possess the SP1 and
69 SP2 spacer peptides and the p6 domain. During maturation, Gag is cleaved by the viral protease into
70 constituent proteins. MA is retained at the viral membrane, NC stays bound with the bi-partite viral
71 genome, and CA reorganizes around the viral genome to form a conical-shaped capsid core.

72

73 HIV-1 CA is composed of two alpha-helical domains connected by a flexible linker [3-5]. Its N-terminal
74 domain (CA_{NTD}) is made of 7 α-helices (H1 to H7) and contains functional domains that bind to cellular
75 factors such as Cyclophilin A (CypA) [3] and TRIM5α [6, 7]. The C-terminal domain (CA_{CTD}) contains
76 4 α-helices (H8 to H11). The function of CA_{CTD} is primarily to form inter-molecular contacts that are
77 important to the stability of immature Gag and mature CA lattice structures and infectivity of the virus.

78

79 In HIV-1 immature particles, the Gag proteins assemble into a hexagonal lattice structure through
80 extensive interactions among the CA proteins [8-13]. The CA protein hexamers adopt a wineglass-like
81 structure to accommodate the spherical shape of the viral membrane. The "bowl" of the wineglass is
82 composed of six copies of CA_{NTD} on the rim and six copies of CA_{CTD} at the bottom of the bowl. The
83 "stem" of the wineglass is a six-helix bundle (6HB) structure that consists of the C-terminal tail of CA
84 and the SP1 segment (CA-SP1) [14]. The 6HB in HIV-1 is further stabilized by the cellular metabolite
85 inositol hexakisphosphate (IP6) that is closely positioned within the positively charged rings of lysine
86 residues in the C-terminal end of CA_{CTD} (K290) and SP1 (K359) [14, 15]. The Gag lattice is stabilized
87 by the molecular interactions of CA_{NTD} (H1 and H2) at local three-fold and two-fold axes respectively
88 and the also CA_{CTD} interactions (H9) at the local two-fold axes [14].

89

90 The HIV-1 capsid core has a fullerene structure composed of approximately 250 CA hexamers and 12
91 pentamers [16, 17]. In contrast to the CA hexamers in the immature lattice, each capsomer in the
92 mature CA lattice adopts a bell-shaped structure. The CA_{NTD} forms the inner ring and the closed end
93 of the bell. The CA_{CTD} forms the outer ring connecting the neighboring capsomers. The HIV-1 CA_{CTD}
94 H10 forms the trimer interface and H9 forms the dimer interface between the adjacent CA molecules.

95

HIV-1 and HIV-2 share 54% amino acid sequence identity between their Gag polyproteins [18]. The crystal structure of HIV-2 CA_{NTD} is the only high-resolution protein structure of HIV-2 CA solved to date (PDB ID: 2WLV) [19]. Little is known about HIV-2 immature Gag assembly. By cryo-electron microscopy (cryo-EM), we demonstrated that the HIV-2 Gag lattice structure has an intrinsic curvature with fewer interspersed gaps than that reported for HIV-1 [9]. To gain insight into the critical interaction interfaces for HIV-2 immature Gag lattice, we determined the structure of Gag hexamer at 5.5 Å resolution by cryo-EM single-particle reconstruction method (SPR). We also solved a 1.98 Å crystal structure of the HIV-2 CA_{CTD}, which revealed a novel extended 3_{10} helix (H12). The H12 and its interaction with H10 in the crystal dimer were found to be critical components for HIV-2 particle infectivity. These findings support a vital interaction of the HIV-2 CA_{CTD} that must remain intact for particle infectivity.

Results

HIV-2 Gag hexamer structure is uniform and independent of the lattice curvature

To understand the molecular structure of the HIV-2 Gag assembly, we acquired and processed cryo-EM images of HIV-2 immature viral-like particles (VLPs) purified from HEK 293T/17 (293T) cells. As shown in our previous publications [20], the ordered Gag lattice densities in these particles occupied an extensively large region underneath the viral membrane. The completeness of the continuous Gag density layer does not seem to be affected by the size of the VLPs suggesting an intrinsic flexibility exists in the HIV-2 Gag lattice structure to comply with the variation of the membrane curvature. We employed standard cryo-EM SPR techniques to extract non-overlapping images at the center of the lattice region of the imaged VLPs. The circumference of each VLP is at a similar defocus, allowing us to rapidly analyze heterogeneous sized VLPs by isolating segments of the Gag lattice along this uniform feature (**Figure 1A**). By enforcing the six-fold rotational symmetry from the hexamer we can obtain enough angular sampling to solve a reconstruction of the underlying capsid lattice. The final reconstruction of the HIV-2 CA lattice was resolved to 5.5 Å resolution that contains 19 hexamer units of the HIV-2 Gag lattice **(Figure 1B-D**).

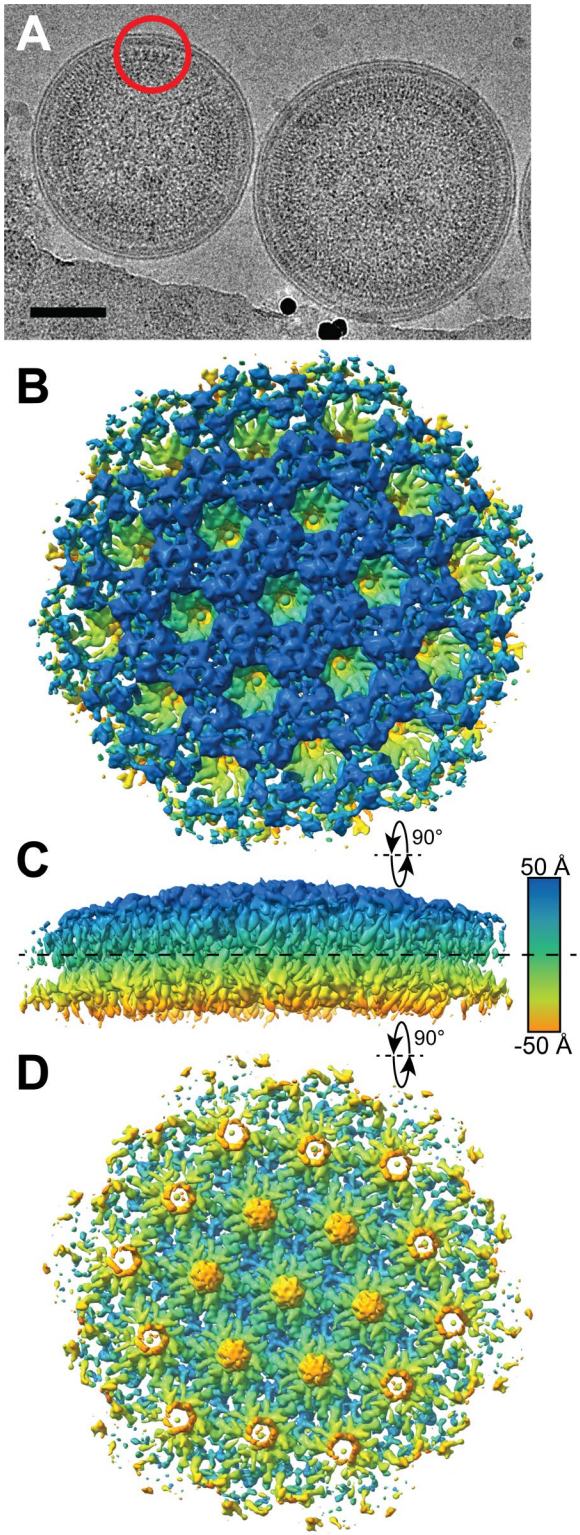

Figure 1. HIV-2 Gag lattice structure from immature particles. (**A**) Cryo-EM micrograph of immature HIV-2 VLPs. Red circle indicates an example area of extracted particles. Scale bar 50 nm. (**B**) Top view, (**C**) side, and (**D**) bottom view of the 5.5 Å reconstruction map showing densities of CA_{NTD} (blue), CA_{CTD} (green) and CA-SP1 (orange). The displayed colors are based on the height of the reconstruction along the z-axis indicated with the color key in (right side - panel C).

132 **Critical components of the HIV-2 hexametric interface are similar to HIV-1**
133 The overall immature HIV-2 Gag structure from VLPs allowed modeling of Gag residues L149 to E371
134 into the density (**Figure 2**). This consisted of CA residues L14 to E236 and SP1 residues A1 to E6.
135 The determined structure of HIV-2 CA molecule in the Gag lattice can be superimposed with that of
136 HIV-1 CA (PDB ID: 5L93) and exhibits a C_{alpha} RMSD of 1.10 Å. Such structural similarity among
137 *lentiviruses* indicates the structural stability of the Gag hexamer as a structural building block of the
138 immature lattice. Similar to HIV-1 or other retroviruses, the HIV-2 CA molecule exhibits two flexible
139 hinge regions. The first hinge region is located between the NTD and CTD (**Figure 2**), which
140 contributes to the structure transformation of CA from the immature Gag lattice conformation to the
141 mature capsid conformation. The second hinge region is located between the H11 and 6HB.
142
143 The regions corresponding to the CA-SP1 domains in the central hexamers is present in the
144 reconstruction. The 6HB densities slightly twist in a right-hand manner. The length of these density
145 layers is ~25 Å, which can accommodate the predicted 13 amino acid residues of the CA-SP1 region
146 (Gag residues P358 to E371). Although the resolution of our reconstruction map is not high enough to
147 determine residue conformations, the overall molecular fitting of our structure indicate a similar
148 structural confirmation to HIV-1. Extra globular shaped densities observed inside the tubular six-helix
149 bundles are attributable to IP6 (**Figure 2A**, red arrow). This observation is consistent to what has
150 been reported to the HIV-1 immature Gag lattice structure [14, 21] and consistent with the finding that
151 IP6 plays a role in HIV-2 immature particle assembly [15].
152
153 The HIV-2 Gag inter-hexamer interface is maintained by two molecular contact regions. One is
154 located at the CTD-CTD interface between H9 at a local 2-fold position (**Figure 2E**). The set of
155 interactions is related to the NTD-NTD interaction via H2 at the local 3-fold position (**Figure 2F**) and
156 between H1 and H6 at the local 2-fold position. These contacts regions are conserved among
157 *lentiviruses*. Based on studies of HIV-1 Gag structure, the critical interactions between H9 are made
158 through residues W184 (HIV-2 W183) and M185 (HIV-2 M184) (Gag sequence: W316 and M317) and
159 are conserved between HIV-1 and HIV-2. Mutational studies in HIV-1 have previously demonstrated
160 that these conserved residues are important to Gag assembly [22, 23].

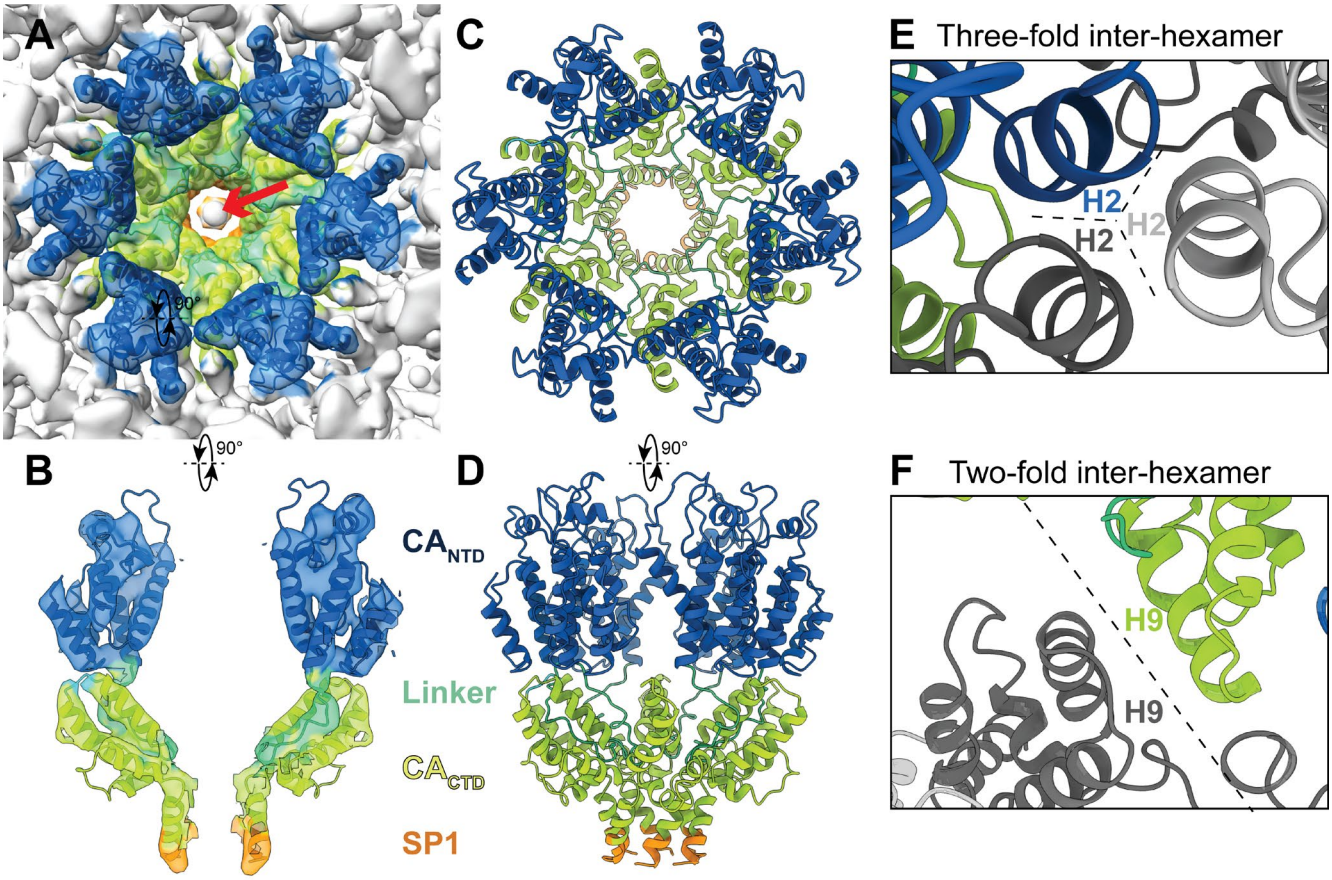

Figure 2. Model of HIV-2 CA hexamer and lattice interfaces. (**A**) Top view of central hexamer reconstruction density fit with the HIV-2 model. The red arrow indicates the IP6 density in the center of the CA_{CTD}. (**B**) Side view of two capsid monomers with density zoned out from a distance of 4 Å from the protein backbone of the central hexamer. (**C**) Top view of HIV-2 hexamer model. (**D**) Side view of HIV-2 hexamer model. (**E**) View of H2 at the three-fold inter-hexamer interface with adjacent hexamers in grey and dark grey. (**F**) View of H9 at the two-fold inter-hexamer interface with adjacent hexamers in dark grey. All models and maps of the central hexamer are colored according to the following capsid regions CA_{NTD} – Blue, Linker (Cyan), CA_{CTD} (Yellow-green), SP1 (Orange).

Crystal structure of HIV-2 CA_{CTD} has a distinct C-terminal alpha helix

To understand the molecular basis of HIV-2 Gag lattice, we expressed and purified the CTD residues 148-231 (HIV-2 CA_{CTD}) to homogeneity for structure determination. HIV-2 CA_{CTD} shares 69% sequence identity with that of HIV-1. This subdomain of HIV-2 CA structure has not been previously solved. HIV-2 CA_{CTD} behaved as a monomer in solution as judged by its size-exclusion chromatography elution profile (data not shown). The purified protein was crystallized, and the structure determined to 1.98 Å resolution (**Figure 3**). The crystal belonged to the space group C2, with one HIV-2 CA_{CTD} molecule in the asymmetric unit forming a dimer via crystallographic dyad symmetry. We were able to model CA residues 148-230 (Gag residues T282 – M365).

181 Similar to other *lentiviral* CA_{CTD} domains [19, 24-26], HIV-2 CA_{CTD} is primarily alpha-helical. Its tertiary
182 structures of the major homology region (MHR), and helix 8 (H8) to helix 11 (H11) superimpose with
183 that HIV-1 CA_{CTD} (PDB ID: 1A43) [26] with backbone C_{alpha} RMSD of 0.74 Å. The dimer interface has
184 two binding regions. The dimerization interface within the HIV-2 CA_{CTD} crystal structure is between
185 H10 and H11 (**Figure 3B**), in contrast, the crystallographic CTD dimer interface in HIV-1 CA_{CTD} is
186 composed of the intermolecular interactions between H9 of each monomer [26]. Specifically, the
187 unique dimeric interface (**Figure 3**) of HIV-2 CA_{CTD} is supported by coordinated electrostatic
188 interactions from the backbone carbonyl group of CTD1-L199 (Gag L334), CTD2-A216 (Gag A351),
189 and CTD2-Q218 (Gag Q353) to the guanidinium group of CTD2-R228 (Gag R363). The second
190 interface is mediated by intermolecular contacts between H10 and an extended C-terminal 3_{10} helix
191 (referred to as helix 12, or H12) (**Figure 3C**). This H12 is in contrast to other retrovirus CA_{CTD} as this
192 portion of the CTD is disordered in the absence of the SP1 peptide in other retroviral CA_{CTD} structures
193 [19, 26]. The angle in which the HIV-2 CA_{CTD} H12 extends from H11 is different from our immature
194 HIV-2 CA lattice from VLPs (**Figure 3D-F**) as well as assembled immature HIV-1 CA-SP1 lattice from
195 VLPs and authentic viral particles [14], or the crystal structure of HIV-1 CA_{CTD}-SP1 dimer (PDB: 5I4T)
196 [19]. In the crystal structure of HIV2 CA_{CTD}, H12 has an acute angle relative to H11 forming the dimer-
197 dimer interface with another CA_{CTD} molecule in the crystallographic unit cell. In the Gag lattice
198 structure, H12 is rotated about 90 degrees and joins SP1 to form a long α-helix in the CA-SP1 helix
199 bundle.
200

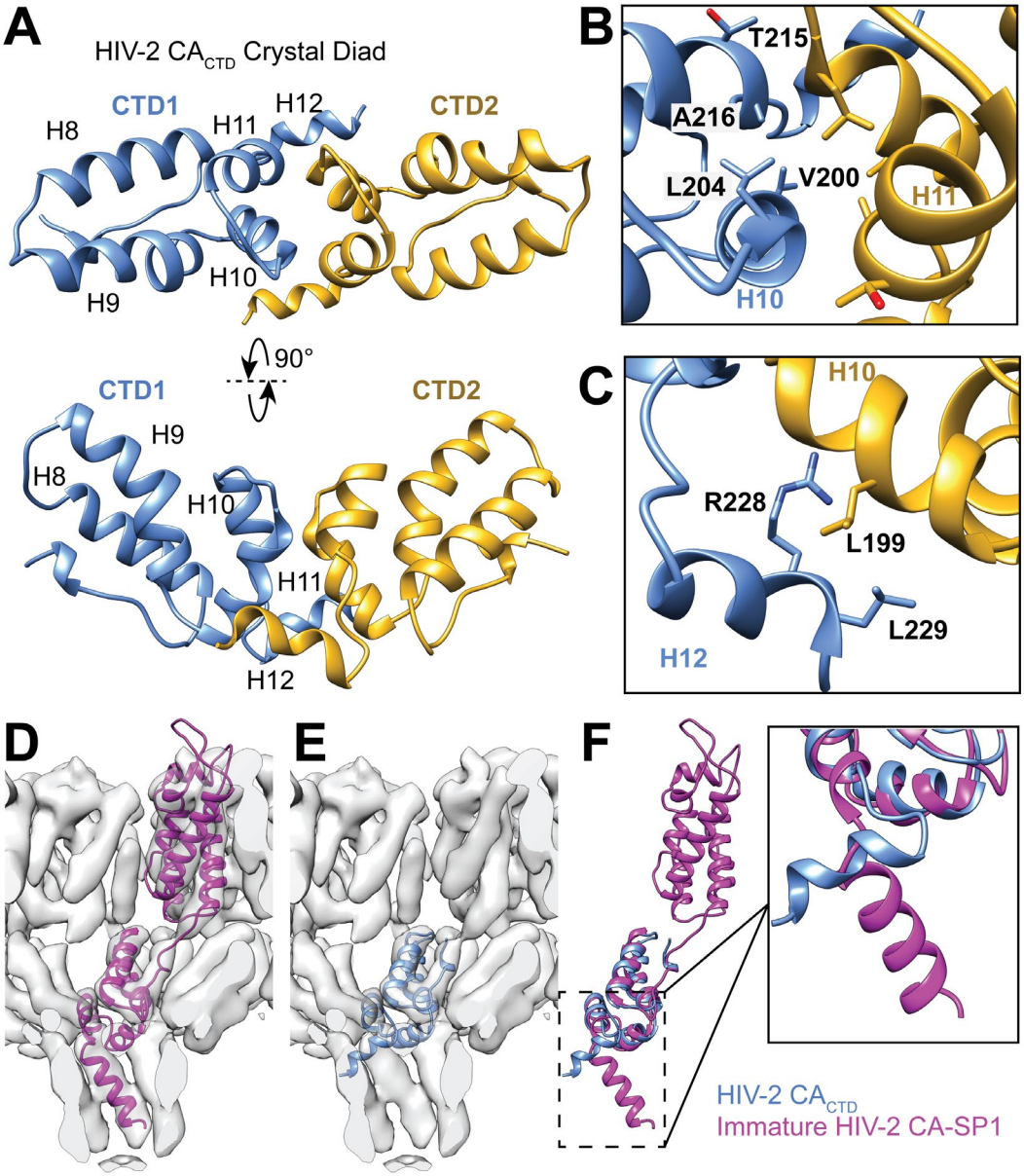

Figure 3. Structure of HIV-2 CA$_{CTD}$ crystal and fitting into immature HIV-2 Gag hexamer. (**A**) The structure HIV-2 CA$_{CTD}$ dimer in a crystallographic unit cell from CA residues 148-230. H8, H9, H10, and H11, represent the four α-helices in HIV-2 CA$_{CTD}$. H12 represents the 3_{10} helix. CTD1 and CTD2 represent two molecules in the dimer. (**B**) Residues V200, L204, A216, T215 located at the H10-H11 crystallographic dimer interface. (**C**) Residues L199, R228 and L229 located at the HIV-2 CA$_{CTD}$ at the H10-H12 crystallographic dimer interface. (**D**) Immature HIV-2 CA model fit into the reconstruction density from immature HIV-2 VLPs. (**E**) HIV-2 CA$_{CTD}$ monomer fit into the reconstruction density from immature HIV-2 VLPs. (**F**) Structural comparison of the immature HIV-2 CA cryo-EM derived model and HIV-2 CA$_{CTD}$ crystal structure showing that H12 of the crystal structure adopts a different conformation of the CA-SP1 helix of the immature CA model.

216 **Mutations to H10 and H12 residues decrease HIV-2 particle infectivity**

217 To determine if the extended HIV-2 H12 has impact on aspects of the retroviral life cycle we made
218 disruptive mutations at critical residues at the H10 and H12 interface. Specifically, residues L199,
219 R228, and R229 were mutated to introduce either modest disruptions (L199G, R228A, and L229G) or
220 strong disruptions (L199K, R228E, and L229K) to the observed CA_{CTD} crystal structure interface
221 (**Figure 3C**). To assess particle assembly defects, we analyzed VLP production from expressing a
222 codon optimized HIV-2 Gag construct harboring the individual mutations in HEK cells. Viral
223 supernatants were assessed via immunoblot for the relative amount of Gag present to WT HIV-2 Gag
224 (**Figure 4A**). Two mutation sites in H12 R228 and L229 showed a significant decrease in produced
225 immature particles where the L199 point mutation showed no significance difference.
226
227 To assess if these mutations had an effect on mature particles, an HIV-2 MIG construct was co-
228 expressed with VSV-G to produce single-cycle mature infectious particles in HEK cells [27]. These
229 particles were used to assess particle production of a more biologically relevant virus particle (**Figure**
230 **4B**). For mature particle production, all the H12 mutations were significantly decreased ~10 to 20 fold
231 compared to the WT virus particles. For the H10 mutation there was a significant decrease to the
232 L199G mutant to ~60% of WT production but the L199K mutation showed no significant difference
233 (**Figure 4B**). The MIG produced HIV-2 pseudovirions that harbor a dual fluorescent reporter were
234 then used to assess particle infectivity by infecting MAGI cells with equivalent amounts of virus as
235 assessed by CA levels in the produced viral supernatant (**Figure 4B**). Specifically, the H10 or H12
236 mutants harboring particles showed significant defects in infectivity as compared to a WT infection.
237 The amount of reporter fluorescence was ~10 to 50 fold less infectious as compared to equivalent
238 amounts of WT HIV-2 particles (**Figure 4C**).
239

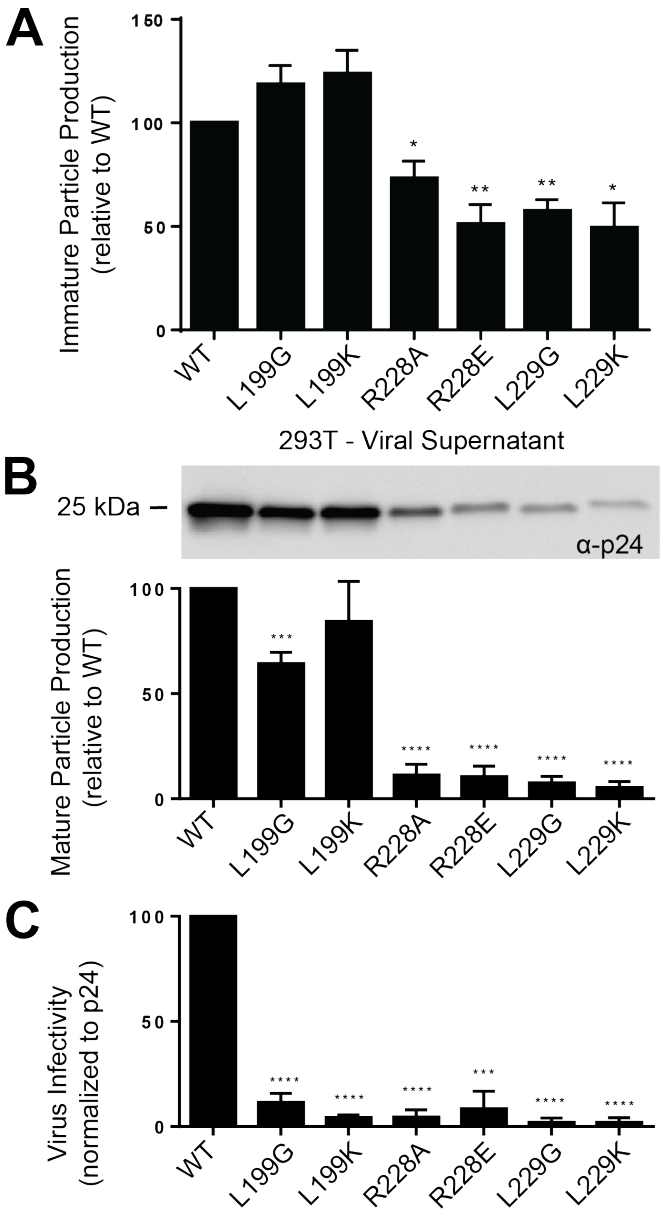

Figure 4. Analysis of mutations in HIV-2 CA_{CTD} H10 and H12 on particle production and infectivity. (**A**) The effect of H10 and H12 mutations on immature particle production, (**B**) mature particle production including an immunoblot of the relative levels of CA (p24) present in the viral supernatant, and (**C**) on particle infectivity is shown. Results are from three independent experiments; average value ± standard error of the mean shown. Significance relative to WT as assessed by using an unpaired t-test. ****, $P < 0.0001$; ***, $P < 0.001$; **, $P < 0.01$; *, $P < 0.05$.

251 ## Discussion

252

253 In this study we solved the immature HIV-2 Gag hexamer structure by the cryo-EM SPR method at
254 5.5 Å resolution. Fitting of HIV-2 CA_{NTD} and CA_{CTD} structures into the resolved density map
255 demonstrated a wineglass-like architecture of the central hexamer that is very similar to HIV-1 [14],
256 equine infectious anemia virus (EIAV) [28] and murine leukemia virus (MLV) [29]. The HIV-2 Gag
257 hexamer is stabilized by conserved residues in H2 at the three-fold inter-hexamer interface, by H9 in
258 the CA_{CTD} and a 6HB formed by the CA-SP1 at the six-fold intra-hexamer interface. We also observe
259 a central pore density between the base of the CA_{CTD} and the 6HB that is consistent with the
260 structural co-factor IP6. This feature corresponding to IP6 is consistent with observations from
261 previously determined retroviral structures. In addition, cell and biochemical data indicate that IP6 is a
262 critical factor in capsid self-assembly. HIV-2 contains conserved lysine residues found within two rings
263 of six lysine residues at the C-terminal end of CA_{CTD} (K292 in HIV-2) and SP1 (K361 in HIV-2) [28, 30,
264 31].

265 HIV-1 and HIV-2 CA proteins share 67% sequence identity. The amino acid variations indicate subtle
266 differences in the chemical environment in their Gag hexamer and lattice structures [32, 33]. At the
267 Gag lattice three-fold interface, we found that exchanging HIV-1 and HIV-2 residues significantly
268 reduced virus particle production, and diminished virus infectivity. Mutations of a non-conserved
269 residue on CA H2, *i.e*. HIV-2 CA G38M and HIV-1 CA M39G reduced virus particle production by
270 50%, and eliminated virus infectivity. The HIV-2 CA N127E mutant, which swaps HIV-1 and HIV-2
271 residue identity, severely reduced particle production [34]. In addition, HIV-2 is insensitive to the HIV-1
272 maturation inhibitor (MI) Bevirimat (BVM) [35]. The binding site of BVM has been determined to be
273 inside the CA-SP1 six-helix bundle near the IP6 binding site [14, 36, 37]. Therefore, it is important to
274 obtain a near-atomic structure of HIV-2 immature Gag lattice to determine its specific chemical
275 environment in those regions compared to that of HIV-1.

276 From our crystal structure of the HIV-2 CA_{CTD}, residues in H10 and H12 play a critical role in
277 mediating the dimeric interface observed in the crystal. The C-terminal residues of HIV-2 CA form a
278 3_{10} helix, H12, in the crystal. This domain shows a poor fit for that region in the immature HIV-2 CA
279 cryo-EM density for CA-SP1 residues. Therefore, further analysis was conducted to assess the
280 biological significance of these residues. Conducting site-directed mutagenesis of residues L199,
281 R228, and L229 in H10 and H12 clearly lead to significant impairment of particle production and
282 infectivity for HIV-2 particles in our assays. This suggests that this novel interaction of H10 and H12 in
283 the HIV-2_{CTD} has implications for HIV biology.

284 To further explain the H10 and H12 mutagenesis observations we conducted a modeling exercise to
285 see if these helices show any potential interaction in the context of a mature capsid lattice. To this
286 end, we docked six copies of the HIV-2 CA_{CTD} into the HIV-1_{CTD} mature lattice from an authentic
287 particle reconstruction (PDB ID: 5MCX) [38] (**Figure 5A-C**). A mature HIV-1 lattice was used as the
288 observed HIV-2 CA_{CTD} H12 formation would be equivalent to a mature CA conformation with a
289 protease cleaved Gag at CA-SP1. Analyzing H12 in the modeled fitting shows that the conformation
290 of the CTD in the HIV-2 crystal structure is positioned to interact with H10 of the adjacent hexamers at
291 the three-fold CA inter-hexamer interface (**Figure 5D**). The implications from our observations of the
292 HIV-2 CA_{CTD} and the role of H12 are focused on CA reorganization during the proteolytic cleavage
293 process and particle maturation. One proposed model of these findings is that the symmetrized Gag
294 lattice is a metastable structure that can adapt to the change of membrane curvature during budding
295 and it is ready to dissemble and reorganize after a series of proteolytic cleavages. In this model HIV-2
296 CA_{CTD} H12 could stabilize a lattice intermediate with inter-hexameric contacts. We have clearly shown
297 that the immature lattice of the HIV-2 has conserved structural properties to that of HIV-1 from our
298 VLP reconstruction. Residues within H12 of HIV-2 CA confer properties of viral infectivity identified
299 from our structural analysis of HIV-2 CA_{CTD} and mutagenesis studies analyzing particle release and
300 infectivity. The mechanistic insights to how this region of CA stabilizes the HIV-2 Gag lattice during
301 maturation should be a focus for further study.

302

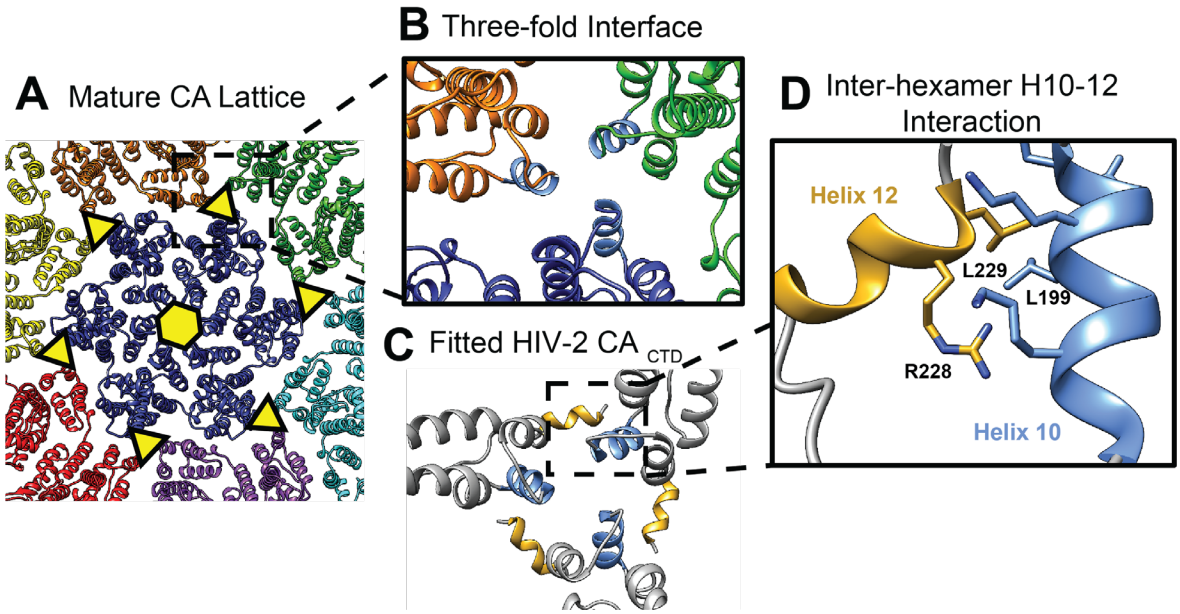

304 **Figure 5: Modeling implications of helix 12 in a mature lattice configuration.** (**A**) Mature HIV-1 lattice (PDB
305 ID: 5MCX) colored by hexamers. Three-fold and 6-fold symmetry interfaces indicated with yellow triangles and
306 hexamer cartoon. (**B**) View of CA_{CTD} of mature HIV-1 three-fold interface with helix 10 indicated in light blue. (**C**)
307 Three copies of HIV-2 CA_{CTD} fit to HIV-1 CA_{CTD} positions. (**D**) View of hypothesized H10-12 interface from this
308 modeling exercise.

309 ## Materials and Methods

310

311 **HIV-2 CA_{CTD} protein purification, crystallization, and structure determination**

312 We expressed HIV-2 CA_{CTD} in *E. coli* strain BL21 (DE3) with a N-terminal 6xHis-tag, using the pET28a
313 expression vector. The expressed protein was purified by Ni-NTA affinity and Superdex 75 size-
314 exclusion chromatography (SEC) steps. The 6xHis-tag was removed by a treatment with HRV 3C
315 protease after elution from the Ni-NTA column and prior to the SEC step. The purified protein in 20
316 mM Tris-HCl (pH 7.4), 0.5 M NaCl, 5 mM β-mercaptoethanol was concentrated by ultrafiltration to ~43
317 mg/ml. Crystallization screening was performed on a Phoenix (Art Robbins Instruments, USA)
318 crystallization robot. Crystals appeared in one day and grew to full size in three days. The crystals that
319 gave the best diffraction were grown with a reservoir solution containing 1.2 M tri-sodium citrate, 0.1
320 M Bis-Tris propane, pH 7.0.

321

322 The HIV-2 CA_{CTD} crystals were cryo-protected by soaking in the crystallization reservoir solution
323 supplemented with 25% ethylene glycol and flash cooled in liquid nitrogen. X-ray diffraction data were
324 collected at the 24-ID-E beam line of the Advanced Photon Source, using the wavelength of 0.979 Å
325 and processed using HKL2000. The crystal structure was solved by the molecular replacement
326 phasing, using the coordinates of the T58A/I124A mutant of the HIV-1 capsid protein (PDB ID: 6AXX)
327 as the search model. Iterative model building and refinement were performed using COOT [39] and
328 PHENIX [40] give a final R_{work} and R_{free} of 22.39% and 24.95%, respectively. The final model consists
329 of 83 amino acids. Refinement and validation metrics are listed in **Table 1**.

330

331 **Immature VLPs production and purification**

332 The HIV-2 Gag gene (bases 1103 to 2668 from GenBank accession number M30502.1) was cloned
333 into a pN3 expression vector that included within a cassette that contains a 5′ Kozak sequence
334 (GCACC**ATG**, start codon in bold). The pN3-gag expression constructs and their homologous
335 envelope glycoprotein (gp160) expression plasmids were co-transfected into 293T/17 or 293f cells
336 using GenJet ver II at a mass ratio of 10:1. After 48-120 hours post-transfection, the cell culture
337 supernatant was harvested and filtered through a 0.22 µm filter. Purification of the particles was
338 conducted by a series of ultracentrifuge steps. Initially, the viral supernatant was pelleted over an 8%
339 (v/v) OptiPrep™ cushion in STE buffer (100 mM NaCl, 10 mM Tris-Cl pH 7.4, 1 mM EDTA) with a 50.2
340 Ti rotor (Beckman Coulter, CA) at 211,400 x g for 90 min. The pellet was resuspended in STE buffer
341 and banded out over an OptiPrep™ step gradient (10, 20, 30% OptiPrep™ (v/v)) with a SW55 Ti rotor
342 (Beckman Coulter, CA) at 211,400 x g for 90 min. The final VLP sample was suspended in STE
343 buffer.

344 **Mature particle production**

345 The HIV-2 *pROD-MIG* plasmid and a VSV-G expression construct were co-transfected into
346 HEK293T/17 cells using GenJet ver II at a 3:1 mass ratio to produce WT and mutant infectious viral
347 particles. After 48-hours post-transfection, the viral supernatants were harvested, clarified by
348 centrifugation (1,800 × g for 10 min), and filtered through 0.2 μm filters. Then the supernatants were
349 concentrated by ultracentrifugation in a 50.2 Ti rotor (Beckman Coulter, CA) at 211,400 × g for 90 min
350 through an 8% OptiPrep™ (Sigma-Aldrich, MO) cushion. The efficiency of mature particle production
351 was analyzed by quantifying the CA (p24) band in culture supernatants using anti-HIV-1 p24 primary
352 antibodies (Santa Cruz Biotechnology, CA - Mouse anti p24: sc-69728) and goat anti mouse
353 StarBright 700 (Bio-Rad, CA). Capsid protein levels were assessed by SDS-PAGE followed by
354 immunoblotting with an anti-HIV-1 CA (p24) antibody. To account for variations in particle production
355 CA levels from mutant viral supernatants were normalized relative to WT for subsequent analysis.

356

357 **Infectivity assay**

358 The HIV-2 *pROD-MIG* plasmids and the VSV-G expression construct were co-transfected into
359 HEK293T/17 cells using GenJet, ver II (SignaGen, Gaithersburg, MD) at a 3:1 ratio to produce WT
360 and mutant infectious viral particles. After 48-hours post-transfection, the viral supernatants were
361 harvested, clarified by centrifugation (1,800 × g for 10 min), and filtered through 0.2 μm filters. U373-
362 MAGI-CXCR4 cells were plated in a 12-well plate and each well treated with 1 ml viral supernatants
363 and 1 mL fresh medium. Each group had 4 well replicates. The cells were collected for fluorescence
364 analysis via BD LSR II flow cytometer (BD Biosciences) 48-hours post-infection as described before
365 (Rawson et al. 2016). Flow cytometry data were examined in FlowJo v.7 (Ashland, OR). The
366 infectious cells were calculated from the flow data by adding all positive quadrants (mCherry+ only,
367 GFP+ only, and mCherry+/GFP+) to determine infectivity. Mutant infection level was determined
368 related to WT. Then, the relative infectivity of each group was normalized to its relative mature particle
369 production as assessed by p24 immunoblot of the produced particles. Three independent experiments
370 were performed.

371

372 **Cryo-EM data collection**

373 The frozen-hydrated TEM grids are prepared by manual blotting in a FEI MARK III Vitrobot system. A
374 small volume (~3.5 μl) of concentrated VLP sample, or VLP mixed with BSA-treated 20nm Nano gold
375 particles, were applied to a glow-discharged quantifoil holey carbon grid (Ted Pella, Redding, CA) and
376 then blotted with a filter paper before being plunged into liquid ethane. The frozen grids were first
377 examined and screened in an in-house FEI TF30 field emission gun transmission electron microscope
378 (TEM) at liquid nitrogen temperature (FEI Company, Hillsboro, OR). The grids were then transported

379 to the National Cryo-EM Facility, Cancer Research Technology Program, Frederick National
380 Laboratory for Cancer Research for high-resolution cryo-EM data collection.
381
382 The cryo-EM data used for image processing were collected on a Titan Krios TEM that was operated
383 at 300 kV in the Nanoprobe EFTEM mode. The images were recorded using a K2 Summit direct
384 electron detector that was positioned post a Gatan BioQuantum energy filter with a 20 eV energy slit
385 for the zero-loss image collection. The cryo-EM movies were recorded at 105,000x nominal
386 magnification, which corresponds to 0.66 Å at the specimen in super resolution mode. Each movie
387 contains 40 frames with an accumulated electron dose of 30-50 $e^-/Å^2$. The defocus levels for the cryo-
388 EM data collection was set to 0.75 to 2.25 µm. The whole data set contains 2508 movies. Movies
389 were motion corrected and dose-weighted using the MotionCor2 program [27]. The contrast transfer
390 function (CTF) parameters were determined using Gctf [41]. Detailed data acquisition parameters are
391 listed in **Table 2**.
392
393 **Single particle reconstruction**
394 Single particle reconstruction was processed in RELION-3.1 [42, 43]. Initially, ~1,000 Gag lattice
395 regions on the edges of the VLP particles centered on the capsid lattice were picked out from 2415
396 micrographs selected that contained ideal CTF parameters. Then 219,321 particles were identified
397 using a template-based auto picking procedure implemented in RELION-3.1 from 2D classes of the
398 manually picked particles. The box size of these local Gag lattice regions is 400 pixels, corresponding
399 to 528 Å on the specimen. The extracted particles were subjected to multiple cycles of 2D
400 classification (remove contaminates and disordered classes) and 3D classification (identify
401 homogenous set of particles). The final reconstruction from a selected 46,017 particles led to a 5.5 Å
402 resolution based on Fourier-shell correlation coefficient cut-off of 0.143.
403
404 **Gag lattice model building and refinement**
405 The HIV-2 CA-SP1 protein structural model is generated from threading the HIV-2 CA sequence over
406 the immature HIV-1 Gag cryo-EM structure (PDB ID: 5L93) [26]. The protein models were generated
407 using by performing iterative cycles of the real-space refinement routines in Phenix [40] and manual
408 perturbations in Coot [39].
409
410 **Data availability**
411 The cryo-EM single particle reconstruction map of the HIV-2 Gag lattice and associated hexamer
412 model will be available in the EMDB and PDB respectably. The refined model of HIV-2 CA_{CTD}
413 structure was also deposited in PBD.

Acknowledgement

This work is supported by NIH grants R01 GM124279 (to L.M. and J.M.), R35 GM118047 (to H.A.). We thank the staff at the National Cryo-EM Facility, Cancer Research Technology Program, Frederick National Laboratory for Cancer Research for high resolution cryo-EM data collection. Parts of this work were carried out in the Characterization Facility, University of Minnesota, which receives partial support from the NSF through the MRSEC (Award Number DMR-2011401) and the NNCI (Award Number ECCS-2025124) programs. X-ray diffraction data were collected at the Northeastern Collaborative Access Team of Advanced Photon Source, which is funded by the NIH (P30 GM124165). N.T. was supported by NIH grants T32 DA007097 and F32 AI150351. W.G.A was supported by NIH grant T32 AI83196.

Author contributions

L.M.M. and W.Z. designed research; N.T. and L.M. purified the HIV-2 virus-like particle samples; N.T. performed cryo-EM reconstructions; K.S. and H.A. solved the crystal structure of HIV-2 CA_{CTD}; H.Y. and W.G.A., performed mutagenesis studies; H.Y. performed infectivity assays; G.Y. wrote several imaging processing software; N.T. performed structural modeling and fitting. All authors contributed either drafting and/or revising the paper.

431 **Table 1. Data collection and refinement statistics.**

432

	HIV-2_{CTD}
Data Collection	
Wavelength (Å)	0.979
Resolution range (Å)	24.4 - 1.98 (2.05 - 1.98)
Space group	C2
Unit cell	
a,b,c (Å)	48.813, 30.919, 46.494
α,β,γ (°)	90, 90.561, 90
Total reflections	13142 (1335)
Unique reflections	4779 (489)
Multiplicity	2.7 (2.7)
Completeness (%)	95.44 (95.66)
I/σ(I)	11.41 (3.29)
R-merge	0.0624 (0.267)
R-meas	0.0762 (0.326)
R-pim	0.0430 (0.185)
$CC_{1/2}$	0.997 (0.963)
Refinement	
Reflections used	4761 (485)
# for R-free	237 (27)
R_{work}	0.2239 (0.3252)
R_{free}	0.2495 (0.3944)
Number of non-hydrogen atoms	659
Macromolecules	644
Solvent	15
Protein residues	83
RMSD	
Bond lengths (Å)	0.003
Bond angles (°)	0.60
Ramachandran plot	
Favored (%)	97.53
Allowed (%)	2.47
Outliers (%)	0.00
Average B-factor	49.45
Macromolecules	49.62
Solvent	42.34

433 Statistics for the highest-resolution shell are shown in parentheses.

434

435

436 **Table 2. Cryo-EM data collection**

437

Imaging Mode	Single Particle
Data Collection	
Microscope	FEI Titan Krios
Voltage (kV)	300
Magnification	105,000 x
Energy-filter (eV)	20
Detector	Gatan K2 Summit
Recording Mode	Super-resolution
Pixel size (Å/pixel)	1.32
Defocus range setting (μm)	-4.0
Total Dose (e^-/Å^2)	50-60
Dose rate (e^-/sec/pixel)	8.7, 5.6
Exposure time (sec)	10.0
Frame number	40
Dataset size	2508 micrographs

438

References

1. Nyamweya, S., et al., *Comparing HIV-1 and HIV-2 infection: Lessons for viral immunopathogenesis.* Rev Med Virol, 2013. **23**(4): p. 221-40.
2. Freed, E.O., *HIV-1 assembly, release and maturation.* Nat Rev Microbiol, 2015. **13**(8): p. 484-96.
3. Gamble, T.R., et al., *Crystal structure of human cyclophilin A bound to the amino-terminal domain of HIV-1 capsid.* Cell, 1996. **87**(7): p. 1285-94.
4. Gamble, T.R., et al., *Structure of the carboxyl-terminal dimerization domain of the HIV-1 capsid protein.* Science, 1997. **278**(5339): p. 849-53.
5. Momany, C., et al., *Crystal structure of dimeric HIV-1 capsid protein.* Nat Struct Biol, 1996. **3**(9): p. 763-70.
6. Li, Y.L., et al., *Primate TRIM5 proteins form hexagonal nets on HIV-1 capsids.* Elife, 2016. **5**.
7. Wagner, J.M., et al., *Mechanism of B-box 2 domain-mediated higher-order assembly of the retroviral restriction factor TRIM5alpha.* Elife, 2016. **5**.
8. Briggs, J.A., et al., *Cryo-electron microscopy reveals conserved and divergent features of gag packing in immature particles of Rous sarcoma virus and human immunodeficiency virus.* J Mol Biol, 2006. **355**(1): p. 157-68.
9. Briggs, J.A., et al., *Structure and assembly of immature HIV.* Proc Natl Acad Sci U S A, 2009. **106**(27): p. 11090-5.
10. Briggs, J.A., et al., *Cryoelectron microscopy of mouse mammary tumor virus.* J Virol, 2004. **78**(5): p. 2606-8.
11. Maldonado, J.O., et al., *Distinct Morphology of Human T-Cell Leukemia Virus Type 1-Like Particles.* Viruses, 2016. **8**(5).
12. Wright, E.R., et al., *Electron cryotomography of immature HIV-1 virions reveals the structure of the CA and SP1 Gag shells.* EMBO J, 2007. **26**(8): p. 2218-26.
13. Yeager, M., et al., *Supramolecular organization of immature and mature murine leukemia virus revealed by electron cryo-microscopy: implications for retroviral assembly mechanisms.* Proc Natl Acad Sci U S A, 1998. **95**(13): p. 7299-304.
14. Schur, F.K., et al., *An atomic model of HIV-1 capsid-SP1 reveals structures regulating assembly and maturation.* Science, 2016. **353**(6298): p. 506-8.
15. Dick, R.A., et al., *Inositol phosphates are assembly co-factors for HIV-1.* Nature, 2018. **560**(7719): p. 509-512.
16. Temple, J., et al., *A snapshot of HIV-1 capsid-host interactions.* Curr Res Struct Biol, 2020. **2**: p. 222-228.
17. Perilla, J.R., et al., *Integrative structural biology of HIV-1 capsid protein assemblies: combining experiment and computation.* Curr Opin Virol, 2021. **48**: p. 57-64.
18. Motomura, K., J. Chen, and W.S. Hu, *Genetic recombination between human immunodeficiency virus type 1 (HIV-1) and HIV-2, two distinct human lentiviruses.* J Virol, 2008. **82**(4): p. 1923-33.
19. Wagner, J.M., et al., *Crystal structure of an HIV assembly and maturation switch.* Elife, 2016. **5**.
20. Martin, J.L., et al., *Distinct Particle Morphologies Revealed through Comparative Parallel Analyses of Retrovirus-Like Particles.* J Virol, 2016. **90**(18): p. 8074-84.

21. Mattei, S., et al., *High-resolution structures of HIV-1 Gag cleavage mutants determine structural switch for virus maturation.* Proc Natl Acad Sci U S A, 2018. **115**(40): p. E9401-E9410.
22. von Schwedler, U.K., et al., *Functional surfaces of the human immunodeficiency virus type 1 capsid protein.* J Virol, 2003. **77**(9): p. 5439-50.
23. Ganser-Pornillos, B.K., et al., *Assembly properties of the human immunodeficiency virus type 1 CA protein.* J Virol, 2004. **78**(5): p. 2545-52.
24. Gres, A.T., et al., *STRUCTURAL VIROLOGY. X-ray crystal structures of native HIV-1 capsid protein reveal conformational variability.* Science, 2015. **349**(6243): p. 99-103.
25. Pornillos, O., B.K. Ganser-Pornillos, and M. Yeager, *Atomic-level modelling of the HIV capsid.* Nature, 2011. **469**(7330): p. 424-7.
26. Worthylake, D.K., et al., *Structures of the HIV-1 capsid protein dimerization domain at 2.6 A resolution.* Acta Crystallogr D Biol Crystallogr, 1999. **55**(Pt 1): p. 85-92.
27. Kavsan, V.M., A.V. Iershov, and O.V. Balynska, *Immortalized cells and one oncogene in malignant transformation: old insights on new explanation.* BMC Cell Biol, 2011. **12**: p. 23.
28. Dick, R.A., et al., *Structures of immature EIAV Gag lattices reveal a conserved role for IP6 in lentivirus assembly.* PLoS Pathog, 2020. **16**(1): p. e1008277.
29. Qu, K., et al., *Structure and architecture of immature and mature murine leukemia virus capsids.* Proc Natl Acad Sci U S A, 2018. **115**(50): p. E11751-E11760.
30. Mallery, D.L., et al., *A stable immature lattice packages IP6 for HIV capsid maturation.* Sci Adv, 2021. **7**(11).
31. Obr, M., F.K.M. Schur, and R.A. Dick, *A Structural Perspective of the Role of IP6 in Immature and Mature Retroviral Assembly.* Viruses, 2021. **13**(9).
32. Meissner, M.E., N. Talledge, and L.M. Mansky, *Molecular Biology and Diversification of Human Retroviruses.* BioRxiv, 2022.
33. Nakanishi, S., et al., *Virological characterization of HIV-1 CA-NTD mutants constructed in a virus-lineage reflected manner.* J Med Invest, 2018. **65**(1.2): p. 110-115.
34. Yang, H., et al., *Human immunodeficiency virus type 2 capsid protein mutagenesis defines the determinants for Gag-Gag interactions.* BioRxiv, 2022.
35. Li, F., et al., *PA-457: a potent HIV inhibitor that disrupts core condensation by targeting a late step in Gag processing.* Proc Natl Acad Sci U S A, 2003. **100**(23): p. 13555-60.
36. Kleinpeter, A.B. and E.O. Freed, *HIV-1 Maturation: Lessons Learned from Inhibitors.* Viruses, 2020. **12**(9).
37. Purdy, M.D., et al., *MicroED structures of HIV-1 Gag CTD-SP1 reveal binding interactions with the maturation inhibitor bevirimat.* Proc Natl Acad Sci U S A, 2018. **115**(52): p. 13258-13263.
38. Mattei, S., et al., *The structure and flexibility of conical HIV-1 capsids determined within intact virions.* Science, 2016. **354**(6318): p. 1434-1437.
39. Emsley, P., et al., *Features and development of Coot.* Acta Crystallogr D Biol Crystallogr, 2010. **66**(Pt 4): p. 486-501.
40. Adams, P.D., et al., *PHENIX: a comprehensive Python-based system for macromolecular structure solution.* Acta Crystallogr D Biol Crystallogr, 2010. **66**(Pt 2): p. 213-21.
41. Zhang, K., *Gctf: Real-time CTF determination and correction.* J Struct Biol, 2016. **193**(1): p. 1-12.

42. Scheres, S.H., *Processing of Structurally Heterogeneous Cryo-EM Data in RELION.* Methods Enzymol, 2016. **579**: p. 125-57.
43. Zivanov, J., et al., *New tools for automated high-resolution cryo-EM structure determination in RELION-3.* Elife, 2018. **7**.